Science Advances

▌AAAS

Supplementary Materials for

Increasing riverine heat influx triggers Arctic sea ice decline and oceanic and atmospheric warming

Hotaek Park*, Eiji Watanabe, Youngwook Kim, Igor Polyakov, Kazuhiro Oshima, Xiangdong Zhang, John S. Kimball, Daqing Yang

*Corresponding author. Email: park@jamstec.go.jp

This PDF file includes:

Description of Methods
Table S1
Figs. S1 to S7
References

Description of Methods

Modeling approach

The CHANGE model includes two modules. The first module represents land surface processes simulating explicit water and energy fluxes, and vegetation dynamics in the atmosphere–soil/permafrost–vegetation system. The second module includes a river discharge scheme adopting a storage-based distributed water routing algorithm with 0.5° resolution for both latitude and longitude (*1, 17*). In the Arctic regions, winds are strong and weather station measurements are sparse, which increase biases in observed precipitation, affecting the quality of the simulated river discharge and T_w, and eventually, Q_{rh} delivered to the Arctic Ocean. Bias in Q_{rh} can propagate to additional uncertainties in model-simulated Arctic sea-ice thickness and extent. To reduce uncertainties associated with any single model forcing, we used three different gridded climatic datasets as inputs for the CHANGE simulations [i.e., WATCH Forcing-Data ERA-Interim (WATCH); http://www.eu-watch.org/data_availability; CRUNCEP - Atmospheric Forcing Data for the Community Land Model (CRUNC), https://rda.ucar.edu/datasets/ds314.3/; and the Global Meteorological Forcing Dataset for land surface modelling from Princeton University (PRINC), http://hydrology.princeton.edu/data.pgf.php. The datasets are available for the 1979–2015 period, while the PRINC is from 1979–2012. The datasets were constructed by combining a suite of global observation-based datasets with different reanalysis (i.e., ERA-Interim and NCEP/NCAR) to reduce biases related to low station density and data gaps. River discharge and T_w, simulated using the CHANGE model, were used as riverine freshwater and heat fluxes in the COCO model experiments, which makes it possible to quantify the sensitivity of sea ice to the associated fluxes.

The COCO model, with 25 km horizontal resolution and 28 hybrid σ–z vertical levels, covers the pan-Arctic region down to 45°N latitude. The model and experimental design, except for the river water discharge, are identical to the physical component of the JAMSTEC model, which was successfully used in previous studies (e.g., *12*). The sea-ice module includes a multi-thickness-category configuration (*33*) with a one-layer thermodynamic formulation (*34*), the linear-remapping method for category transfer (*35*), and the elastic–viscous–plastic rheology (*36*). The ocean module is a free-surface ocean general circulation model formulated with the UTOPIA/QUICKEST advection scheme (*37*) and the turbulence closure scheme (*38*) for the surface mixed layer. The model spin-up was initiated with no sea ice, no ocean current, and temperature and salinity fields of the Polar Science Center Hydrographic

Climatology (PHC) version 3.0 (*39*) and conducted for ten years under atmosphere conditions in 1979. The decadal experiment from 1979 to 2015 was then performed. The atmospheric forcing components were constructed from the Climate Forecast System Reanalysis (CFSR: 1979–2010) and version 2 (CFSv2: 2011–2015) 6 hourly dataset of the National Centers for Environmental Prediction (NCEP) (*32*). The Bering Strait throughflow was defined from idealized seasonal cycles of velocity, temperature, and salinity derived from mooring-based estimates (*40*). The same water volume of the Bering Strait throughflow was removed from an Atlantic-side marginal region of the model domain, where a sponge boundary condition was applied: the horizontal diffusion coefficient was enlarged by an order of magnitude, and the temperature and salinity at all ocean depths were restored to the PHC (*39*) monthly mean values.

Two sets of model experiments using the COCO–CHANGE framework were performed. The first (control) experiment used river discharge without consideration of riverine heat (i.e., freshwater input only). In this case, T_w is assumed to be the same as T_s so that riverine heat flux referenced to T_s at each river mouth was kept to zero. The simulated ocean temperature is thus not changed directly by river discharge. The second experiment used the same atmospheric forcing and model configuration as the control, except that the COCO model used variable T_w derived from CHANGE (i.e., the riverine heat flux is positive in most periods). Differences between the two experiments were used to quantify the effect of Q_{rh} on the state of the Arctic atmosphere–sea ice–ocean system in the defined six target regions on the Arctic shelf (Fig. 1C).

Validation of model performance

After spin-up, the COCO model adjusts to the variable climate conditions, which likely increases uncertainties in the first-year (1979) simulation results; therefore, the 1979 model results were excluded from our analyses. Sea-ice extent from CFSR (https://climatedataguide.ucar.edu/climate-data/climate-forecast-system-reanalysis-cfsr) and sea-ice thickness from satellite observations (http://www.cpom.ucl.ac.uk/csopr/seaice.html) were used to evaluate the associated model simulations. Regions for model evaluation were defined following our choice of the six target regions on the Arctic shelf (Fig. 1C). However, the quality of simulated sea-ice thickness and extent was evaluated at the pan-Arctic scale since variability of sea-ice area is mainly linked to fluctuations in atmospheric temperature (*41*) and the shelf seas for the analysis have almost opened in September. The validation was conducted for the 2010–2015 period when the sea-ice thickness observations were available. The model simulated thicker ice in the late winter compared to the

observations, while generally capturing seasonal ice decay and growth (fig. S7a). The simulated sea-ice extent shows good agreement with the seasonal variability derived from the observations (fig. S7b), indicating that the model was generally effective in representing sea-ice breakup and freezing periods (3). Further validation of the COCO model was described in a previous study (12).

Role of riverine heat in atmosphere warming

Anomalous ocean heat released to the atmosphere caused warming of the atmospheric surface layer over the Arctic shelf seas. The increase of atmosphere temperature ($\triangle T$) caused by the ocean-atmosphere heat exchange (Q_{ao}) is calculated as

$$\Delta T = Q_{ao}/(\rho \cdot C_p \cdot A \cdot \Delta h)$$

where ρ is the air density (kg m^{-3}), C_p = 1004.64 J kg^{-1} K^{-1} is the specific heat of air, A = 5.183×10^{12} m^2 is the area of six Arctic shelf regions (Fig. 1c), and $\triangle h$ = 300 m is the height of the atmospheric boundary layer in summer (JJAS) (24).

Freezing/thawing date analysis

The satellite observed data were used to examine influences of Q_{rh} on the dates of sea-ice breakup in spring and freezing in autumn, and the resultant open water period. Observational trends in the timing and duration of the non-frozen season across the pan-Arctic basin and Alaska land areas were obtained from an established Freeze/Thaw Earth system data record (FT-ESDR; https://nsidc.org/data/nsidc-0477). The FT-ESDR is derived from calibrated, overlapping satellite microwave brightness temperature (37 GHz) retrievals and defines the predominant frozen or non-frozen condition of the land surface within each 25 km resolution grid cell over a global domain and long-term (from 1979) daily record (42). Primary spring thawing/breakup dates were defined for each year of record as the first day when 12 out of 15 consecutive days between January and August were classified as thawed (42). The primary autumn freezing date was determined when 12 of 15 consecutive days were classified as frozen between September and December. The non-frozen, ice-free season length over land was defined annually as the period between FT-ESDR derived spring thawing/breakup and autumn freezing dates.

Sea-ice concentration (SIC) observations (https://nsidc.org/data/nsidc-0051) were used to classify similar sea-ice FT dynamics over the Arctic ocean, with freezing status defined where SIC >15%. The same majority approach was applied to the FT-ESDR and SIC records to define spring thawing/breakup, autumn freezing, and annual ice-free season over the pan-Arctic land and ocean domains (fig. S1). In the analysis,

temporal gaps in SIC were filled using temporally adjacent observations for each grid cell.

Table S1. **Model uncertainty of riverine heat impacts on sea ice and energy flux.**
Averaged riverine heat discharged to the Arctic Ocean (Q_{rh}), sea-ice volume reduction
caused by Q_{rh} (AIV), and components of anomalous atmospheric heat release (Q_{sw}: net
shortwave radiation, Q_{lw}: upward longwave radiation, Q_{sh}: sensible heat, Q_{le}: latent
heat) and ocean heat content (Q_{ow}) in the upper 100 m driven by Q_{rh} during 1980–2015
based on the three sensitivity experiments. The individual details of the three sensitivity
experiments were described in the Method section.

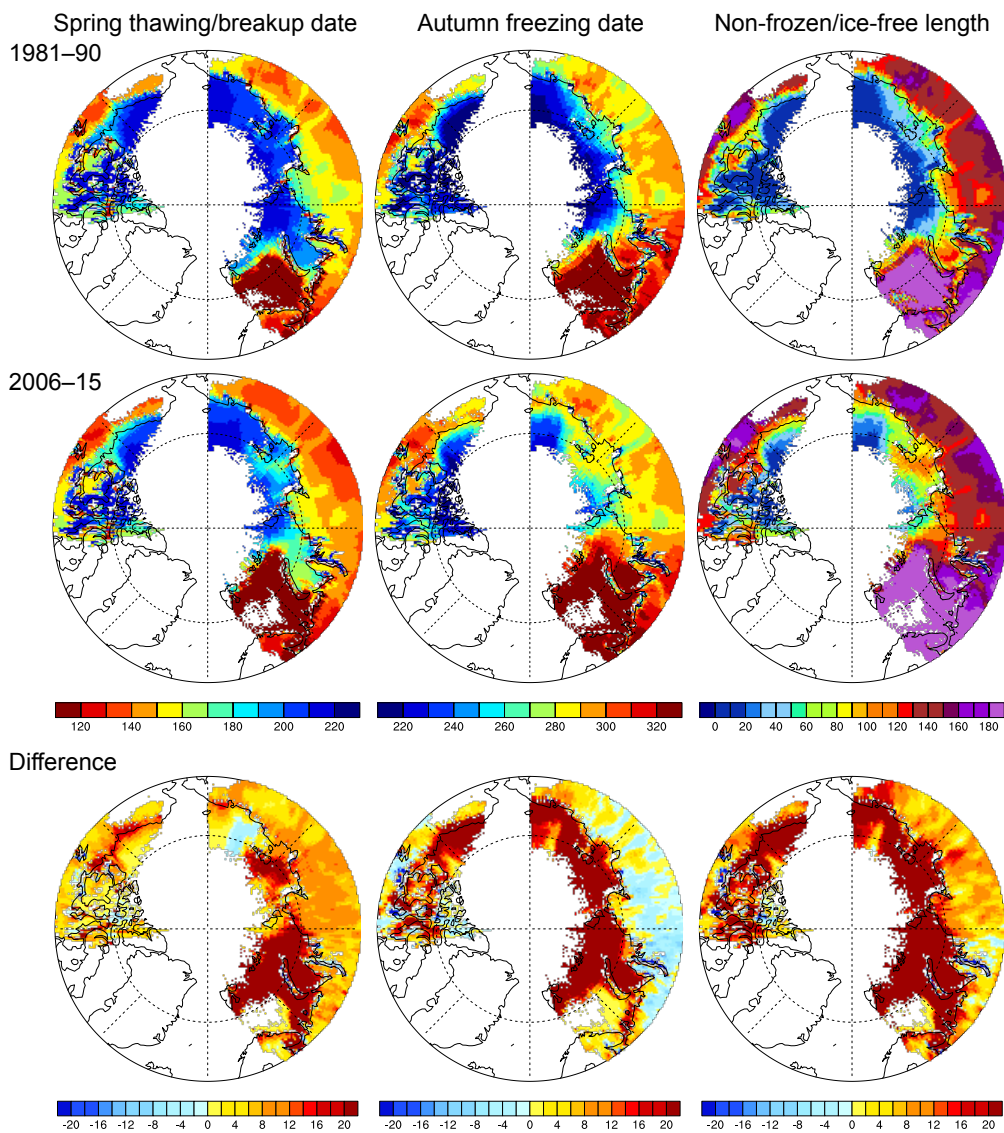| Experiment	Q_{rh}	AIV	Heat				Q_{ow}
			Q_{sw}	Q_{lw}	Q_{sh}	Q_{le}	
	($\times 10^{18}$ J)	(km³)	($\times 10^{18}$ J)				($\times 10^{18}$ J)
CRUNC	81.9	55.7	57.7	28.3	34.9	37.2	44.6
PRINC	100.0	67.7	62.2	32.1	40.9	43.6	48.9
WATCH	101.6	68.8	62.0	32.6	41.1	44.3	50.9
Mean	94.4	63.3	60.6	31.1	39.0	41.9	48.2

Figure S1. **Decadal shifts in observed breakup and freezing dates and annual ice-free period.**

Distribution of averaged spring thawing/breakup date, autumn freezing date (Julian Day), and the length of non-frozen/ice-free season (days) in two decadal periods over the pan-Arctic land and ocean shelf system, and their differences [(2006–15) – (1982–90)]. The positive values in the difference maps represent earlier thawing/breakup, later freezing, and longer non-frozen/ice-free season, respectively. Satellite based sea-ice concentration and landscape freeze/thaw observational records were used to determine the seasonal metrics. White colored areas in the maps represent permanent ice and snow cover, large inland water bodies, open ocean and other areas outside of the targeted modeling domain for this study.
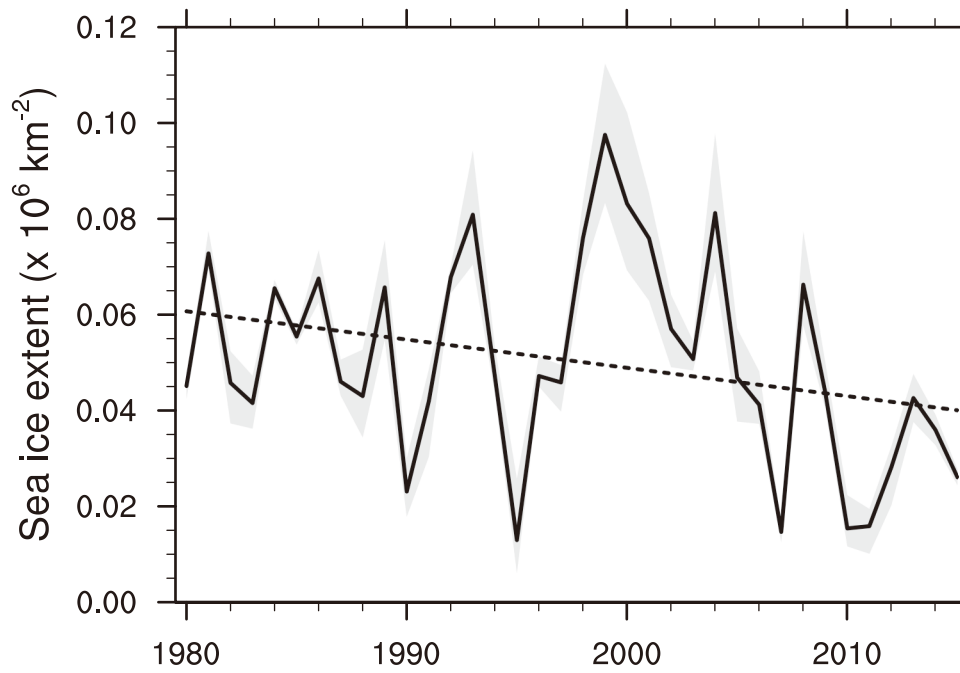
Figure S2. **Variability of riverine heat induced reduction of sea-ice extent in September.**

Decay of September mean sea-ice extent caused by riverine heat over the six Arctic shelf regions. Uncertainty is shown by grey shading evaluated from the three sensitivity experiments (Supplementary). The linear trend is shown by the dotted line.
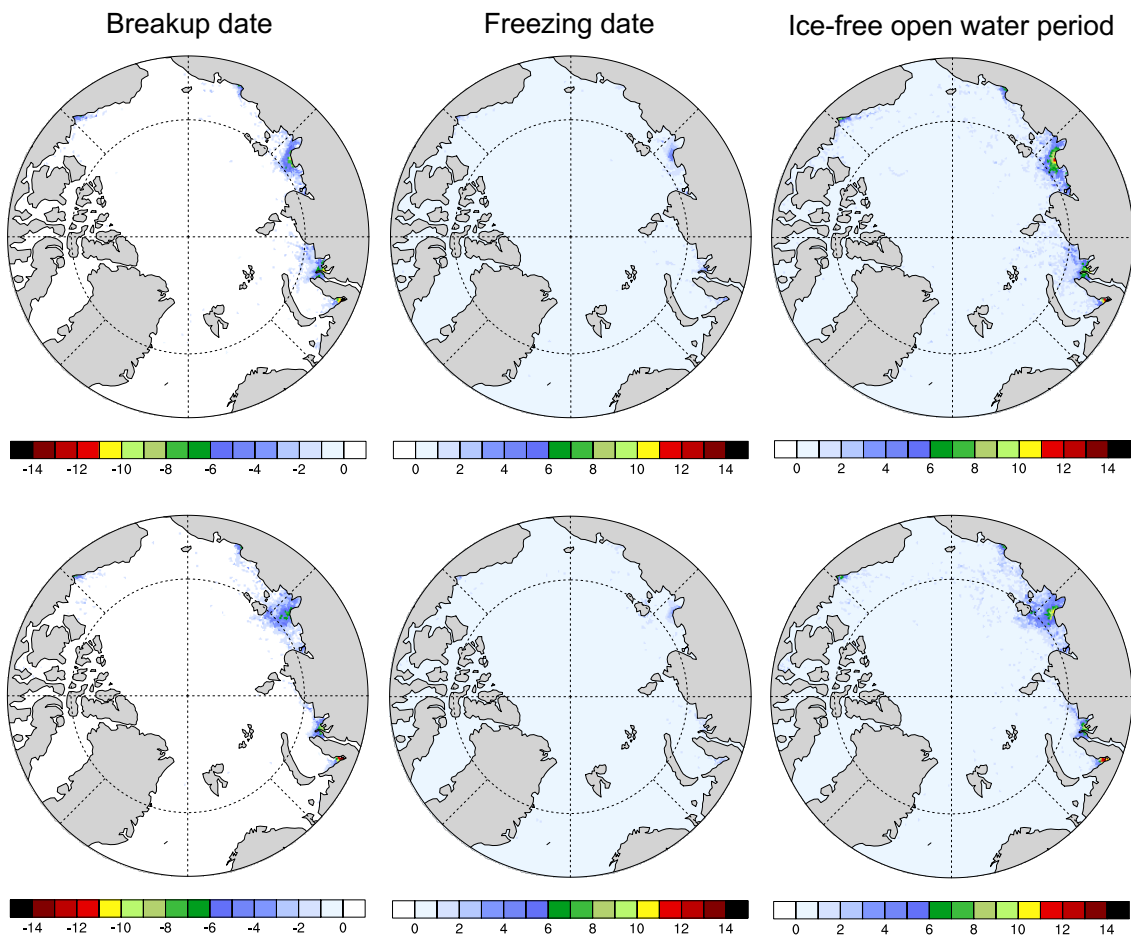
Figure S3. **Anomalous sea-ice breakup and freezing dates and ice-free period caused by riverine heat**.

Spatial distributions of differences (days) in model estimated spring breakup and autumn freezing dates, and annual ice-free open water period averaged for 1981–1990 (top) and 2006–2015 (bottom).
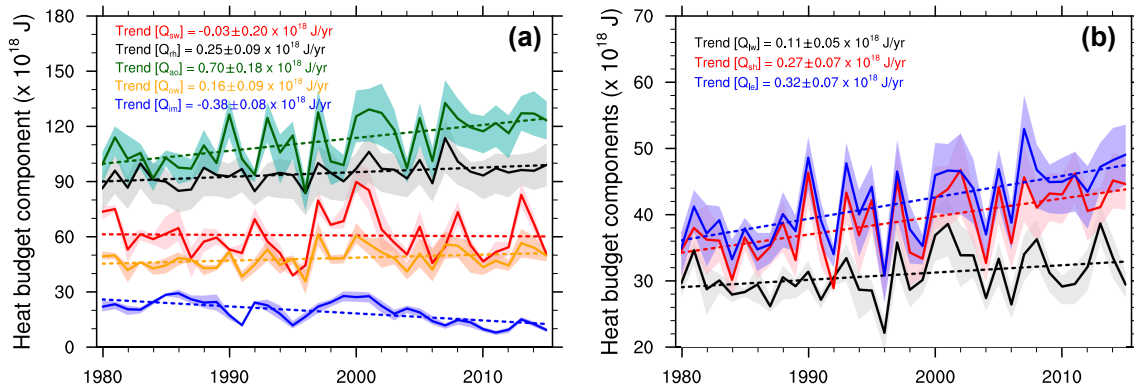
Figure S4. **Variability of riverine heat induced anomalous energy fluxes.**
(a) Ocean heat budget trends including energy sources from riverine heat Q_{rh} and additional absorption of shortwave radiation (Q_{sw}) caused by Q_{rh}, and heat sinks expressed as ocean warming (Q_{ow}), ice melting (Q_{im}), and heat release from ocean to atmosphere (Q_{ao}). (b) Time series of components of Q_{ao} consisting of net upward longwave radiation (Q_{lw}), sensible heat (Q_{sh}), and latent energy (Q_{le}). Linear trend of individual variables is shown by dotted lines, complemented by their values.
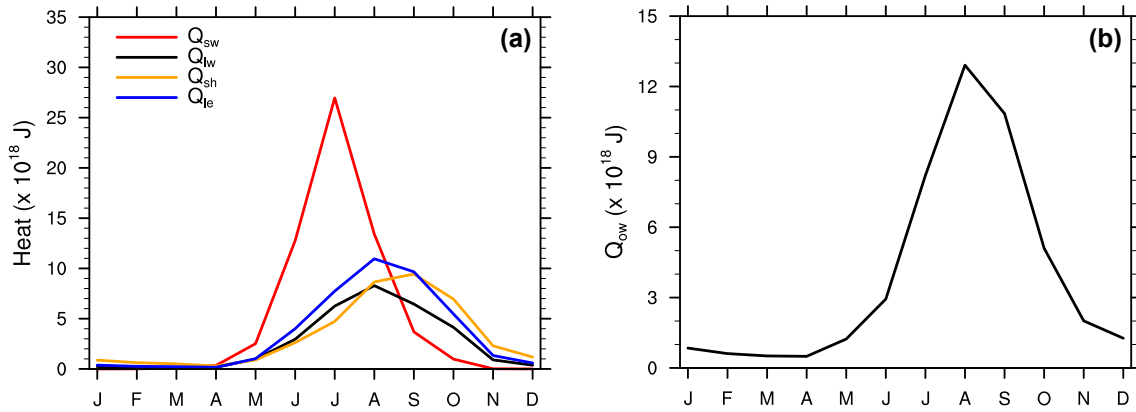
Figure S5. **Seasonal variations of riverine heat induced anomalous energy fluxes.** Seasonal cycle of (a) Q_{rh}-induced anomalous absorption of shortwave radiation (Q_{sw}), outward longwave radiation (Q_{lw}), sensible (Q_{sh}), and latent heat (Q_{le}) and (b) heat associated with ocean warming (Q_{ow}) in the 0–100 m water column averaged over the six Arctic shelf regions for 1980–2015.
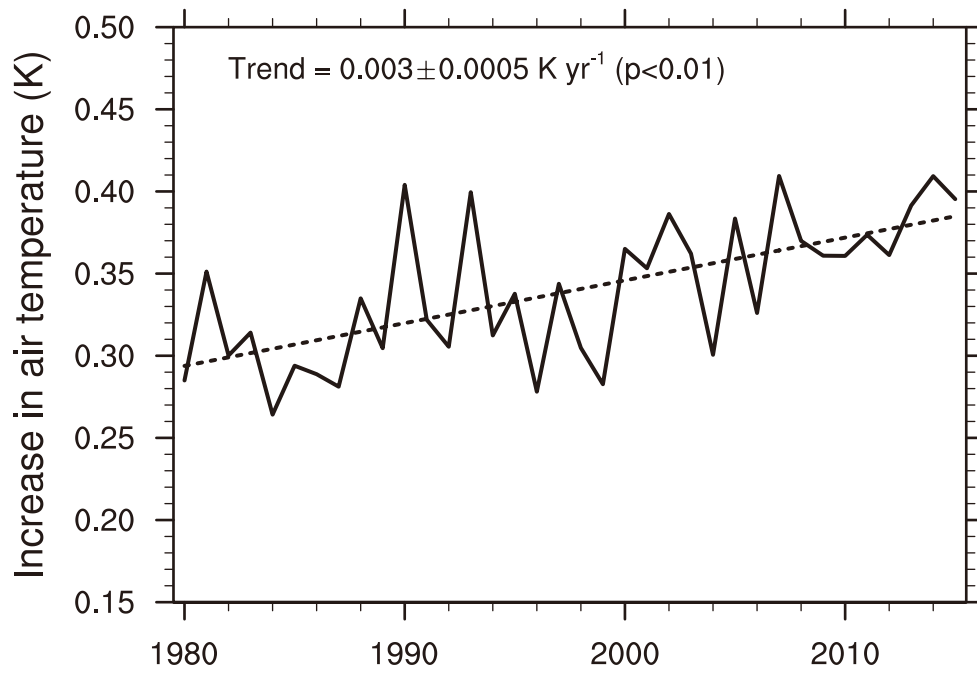
Figure S6. **River heat derived increases of summer air temperature.**
Increase of summer (JJAS) air temperature in the 300 m thick atmosphere boundary layer caused by riverine heat influx (linear trend denoted by dotted line) (Supplementary).
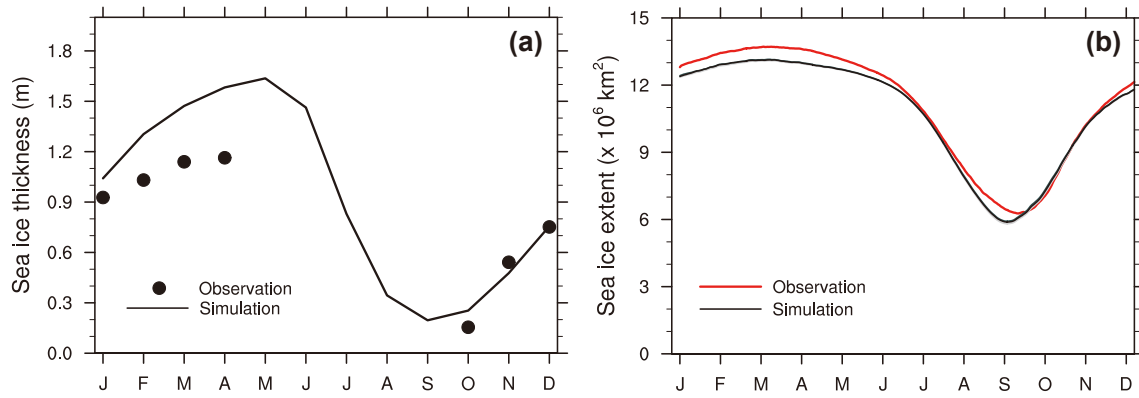
Figure S7. **Validation of model sea ice calculations against observations.**
Comparison of the simulated and observed (Supplementary) sea ice (a) thickness and
(b) extent averaged over the six Arctic shelf domains for the 2010–2015 period.

REFERENCES AND NOTES

1. H. Park, Y. Yoshikawa, D. Yang, K. Oshima, Warming water in Arctic terrestrial rivers under climate change. *J. Hydrometeorol.* **18**, 1983–1995 (2017)

2. R. B. Lammers, J. W. Pundsack, A. I. Shiklomanov, Variability in river temperature, discharge, and energy flux from the Russian pan-Arctic landmass. *J. Geophys. Res.* **112**, G04S59 (2007)

3. M. Janout, J. Hölemann, B. Juhls, T. Krumpen, B. Rabe, D. Bauch, C. Wegner, H. Kassens, L. Timokhov, Episodic warming of near-bottom waters under the Arctic sea ice on the central Laptev Sea shelf. *Geophys. Res. Lett.* **43**, 264–272 (2016)

4. K. G. Dean, W. J. Stringer, K. Ahlnas, C. Searcy, T. Weingartner, The influence of river discharge on the thawing of sea ice, Mackenzie River Delta: Albedo and temperature analyses. *Polar Res.* **13**, 83–94 (1994)

5. S. V. Nghiem, D. K. Hall, I. G. Rigor, P. Li, G. Neumann, Effects of Mackenzie River discharge and bathymetry on sea ice in the Beaufort Sea. *Geophys. Res. Lett.* **41**, 873–879 (2014)

6. E. Carmack, I. Polyakov, L. Padman, I. Fer, E. Hunke, J. Hutchings, J. Jackson, D. Kelley, R. Kwok, C. Layton, H. Melling, D. Perovich, O. Persson, B. Ruddick, M.-L. Timmermans, J. Toole, T. Ross, S. Vavrus, P. Winsor, Toward quantifying the increasing role of oceanic heat in sea ice loss in the new Arctic. *Bullet. Amer. Meteor. Soc.* **96**, 2079–2105 (2015)

7. V. M. Kattsov, J. E. Walsh, Twentieth-century trends of Arctic precipitation from observational data and a climate model simulation. *J. Climate* **13**, 1362–1370 (2000)

8. M. C. Serreze, A. P. Barrett, J. C. Stroeve, D. N. Kindig, M. M. Holland, The emergence of surface-based Arctic amplification. *Cryosphere* **3**, 11–19 (2009)

9. J. W. Weatherly, J. E. Walsh, The effects of precipitation and river runoff in a coupled ice-ocean model of the Arctic. *Climate Dynam.* **12**, 785–798 (1996)

10. T. L. Delworth, A. J. Broccoli, A. Rosati, R. J. Stouffer, V. Balaji, J. A. Beesley, W. F. Cooke, K. W. Dixon, J. Dunne, K. A. Dunne, J. W. Durachta, K. L. Findell, P. Ginoux, A. Gnanadesikan, C. T. Gordon, S. M. Griffies, R. Gudgel, M. J. Harrison, I. M. Held, R. S. Hemler, L. W. Horowitz, S. A. Klein, T. R. Knutson, P. J. Kushner, A. R. Langenhorst, H.-C. Lee, S.-J. Lin, J. Lu, S. L. Malyshev, P. C. D. Milly, V. Ramaswamy, J. Russell, M. D. Schwarzkopf, E. Shevliakova, J. J. Sirutis, M. J. Spelman, W. F. Stern, M. Winton, A. T.

Wittenberg, B. Wyman, F. Zeng, R. Zhang, GFDL's CM2 global coupled climate models. Part I: Formulation and simulation characteristics. *J. Climate* **19**, 643–674 (2006)

11. A. Nummelin, M. Ilicak, C. Li, L. H. Smedsrud, Consequences of future increased Arctic runoff on Arctic Ocean stratification, circulation, and sea ice cover. *J. Geophys. Res. Oceans* **121**, 617–637 (2016)

12. E. Watanabe, M. Jin, H. Hayashida, J. Zhang, N. Steiner, Multi-model intercomparison of the Pan-Arctic ice-algal productivity on seasonal, interannual, and decadal timescales. *J. Geophys. Res. Oceans* **124**, 9053–9084 (2019)

13. X. Zhang, J. Zhang, Heat and freshwater budgets and their pathways in the Arctic Mediterranean in a coupled Arctic Ocean/Sea-ice model. *J. Oceanogr.* **57**, 207–234 (2001)

14. G. Madec; the NEMO team, NEMO ocean engine, in *Note du Pole de Modelisation* [Institut Pierre-Simon Laplace (IPSL), France, 2016].

15. J. Whitefield, P. Winson, J. McClelland, D. Menemenlis, A new river discharge and river temperature climatology data set for the pan-Arctic region. *Ocean Model.* **88**, 1–15 (2015)

16. H. Hasumi, CCSR Ocean Component Model (COCO) version 4.0, in *Center for Climate System Research Report* (University of Tokyo, 2006), vol. **25**, p. 103

17. H. Park, Y. Yoshikawa, K. Oshima, Y. Kim, T. Ngo-Duc, J. S. Kimball, D. Yang, Quantification of warming climate-induced changes in terrestrial Arctic river ice thickness and phenology. *J. Climate* **29**, 1733–1754 (2016)

18. R. A. Woodgate, T. J. Weingartner, R. Lindsay, Observed increases in Bering Strait oceanic fluxes from the Pacific to the Arctic from 2001 to 2011 and their impacts on the Arctic Ocean water column. *Geophys. Res. Lett.* **39**, L24603 (2012)

19. M. A. Rawlins, K. C. McDonald, S. Frolking, R. B. Lammers, M. Fahnestock, J. S. Kimball, C. J. Vörösmarty, Remote sensing of snow thaw at the pan-Arctic scale using the SeaWinds scatterometer. *J. Hydrol.* **312**, 294–311 (2005)

20. Y. Kim, J. S. Kimball, J. Glassy, J. Du, An extended global Earth system data record on daily landscape freeze-thaw status determined from satellite passive microwave remote sensing. *Earth Syst. Sci. Data* **9**, 133–147 (2017)

21. J. A. Curry, J. L. Schramm, E. E. Enert, Sea ice-albedo climate feedback mechanism. *J. Climate* **8**, 240–247 (1995)

22. D. K. Perovich, J. A. Richter-Menge, K. F. Jones, B. Light, B. C. Elder, C. Polashenski, D. Laroche, T. Markus, R. Lindsay, Arctic sea-ice melt in 2008 and the role of solar heating. *Ann. Glaciol.* **52**, 355–359 (2011)

23. I. V. Polyakov, A. V. Pnyushkov, M. B. Alkire, I. M. Ashik, T. M. Baumann, E. C. Carmack, I. Goszczko, J. Guthrie, V. V. Ivanov, T. Kanzow, R. Krishfield, R. Kwok, A. Sundfjord, J. Morison, R. Rember, A. Yulin, Greater role for Atlantic inflows on sea-ice loss in the Eurasian Basin of the Arctic Ocean. *Science* **356**, 285–291 (2017)

24. I. M. Brooks, M. Tjernstrom, P. O. G. Persson, M. D. Shupe, R. A. Atkinson, G. Canut, C. E. Birch, T. Mauritsen, J. Sedlar, B. J. Brookes, The turbulent structure of the Arctic summer boundary layer during the Arctic summer cloud-ocean study. *J. Geophys. Res.* **122**, 9685–9704 (2017)

25. R. V. Bekryaev, I. V. Polyakov, V. A. Alexeev, Role of polar amplification in long-term surface air temperature variations and modern Arctic warming. *J. Climate* **23**, 3888–3906 (2010)

26. P. Schlosser, D. Bauch, R. Fairbanks, G. Bönisch, Arctic river-runoff: Mean residence time on the shelves and in the halocline. *Deep Sea Res. Part I* **41**, 1053–1068 (1994)

27. D. J. Nicolsky, N. Shakhova, Modeling sub-sea permafrost in the East Siberian Arctic shelf: The Laptev Sea region. *J. Geophys. Res.* **117**, F03028 (2012)

28. N. Shakhova, I. Semiletov, A. Salyuk, V. Yusupov, D. Kosmach, Ö. Gustafsson, Extensive methane venting to the atmosphere from the sediments of the East Siberian Arctic shelf. *Science* **327**, 1246–1250 (2010)

29. C. G. Fichot, K. Kaiser, S. B. Hooker, R. M. W. Amon, M. Babin, S. Bélanger, S. A. Walker, R. Benner, Pan-Arctic distributions of continental runoff in the Arctic Ocean. *Sci. Rep.* **3**, 1053 (2013)

30. D. L. Kirchman, X. A. G. Morán, H. Ducklow, Microbial growth in the polar oceans–role of temperature and potential impact of climate change. *Nat. Rev. Microbiol.* **7**, 451–459 (2009)

31. D. Piepenburg, Recent research on Arctic benthos: Common notions need to be revised. *Polar Biol.* **28**, 733–755 (2005)

32. S. Saha, S. Moorthi, H.-L. Pan, X. Wu, J. Wang, S. Nadiga, P. Tripp, R. Kistler, J. Woollen, D. Behringer, H. Liu, D. Stokes, R. Grumbine, G. Gayno, J. Wang, Y.T. Hou, H.-Y. Chuang, H.-M. H. Juang, J. Sela, M. Iredell, R. Treadon, D. Kleist, P. van Delst, D. Keyser, J. Derber,

M. Ek, J. Meng, H. Wei, R. Yang, S. Lord, H. van den Dool, A. Kumar, W. Wang, C. Long, M. Chelliah, Y. Xue, B. Huang, J.-K. Schemm, W. Ebisuzaki, R. Lin, P. Xie, M. Chen, S. Zhou, W. Higgins, C.-Z. Zou, Q. Liu, Y. Chen, Y. Han, L. Cucurull, R. W. Reynolds, G. Rutledge, M. Goldberg, The NCEP climate forecast system reanalysis. *Bull. Am. Meteorol. Soc.* **91**, 1015–1058 (2010)

33. S. Bacon, Y. Aksenov, S. Fawcett, G. Madec, Arctic mass, freshwater and heat fluxes: methods and modelled seasonal variability. *Phil. Trans. R. Soc. A* **373** 20140169 (2015)

34. C. M. Bitz, M. M. Holland, A. J. Weaver, M. Eby, Simulating the ice-thickness distribution in a coupled climate model. *J. Geophys. Res.* **106**, 2441–2463 (2001)

35. C. M. Bitz, W. H. Lipscomb, An energy-conserving thermodynamic model of sea ice. *J. Geophys. Res.* **104**, 15669–15677 (1999)

36. W. H. Lipscomb, Remapping the thickness distribution in sea ice models. *J. Geophys. Res.* **106**, 13989–14000 (2001)

37. B. P. Leonard, M. K. MacVean, A. P. Lock, The flux-integral method for multi-dimensional convection and diffusion, in *NASA Tech. Memo* (NASA, 1994).

38. Y. Noh, H. J. Kim, Simulations of temperature and turbulence structure of the oceanic boundary layer with the improved near-surface process. *J. Geophys. Res.* **104**, 15621–15634 (1999)

39. M. Steele, R. Morley, W. Ermold, PHC: A global ocean hydrography with a high-quality Arctic Ocean. *J. Climate* **14**, 2079–2087 (2001)

40. R. A. Woodgate, K. Aagaard, T. J. Weingartner, Monthly temperature, salinity, and transport variability of the Bering Strait through flow. *Geophys. Res. Lett.* **32**, L04601 (2005)

41. D. Olonscheck, T. Mauritsen, D. Notz, Arctic sea-ice variability is primarily driven by atmospheric temperature fluctuations. *Nat. Geosci.* **12**, 430–434 (2019)

42. Y. Kim, J. S. Kimball, J. Glassy, K. C. McDonald, *MEaSUREs Global Record of Daily Landscape Freeze/Thaw Status, Version 4. Boulder, Colorado USA* (NASA National Snow and Ice Data Center Distributed Active Archive Center, 2017); https://doi.org/10.5067/MEASURES/CRYOSPHERE/nsidc-0477.004.